Energy loss of protons in Au, Pb, and Bi using relativistic wave functions

C. C. Montanari,* C. D. Archubi, D. M. Mitnik, and J. E. Miraglia
Instituto de Astronomía y Física del Espacio, Casilla de Correo 67, Sucursal 28, C1428EGA Buenos Aires, Argentina
and Departamento de Física, Facultad de Ciencias Exactas y Naturales, Universidad de Buenos Aires, Buenos Aires, Argentina
(Received 5 February 2009; published 31 March 2009)

We present a theoretical study on proton energy loss in solid targets of atomic number greater than 54. Fully relativistic wave functions and binding energies are obtained by solving numerically the Dirac equation. *Ab initio* calculations are developed for the first (stopping) and second (straggling) moments of the energy transferred from the ion to the target electrons. The shellwise local plasma approximation is employed for the inner shells, and the Mermin dielectric function is employed for the valence electrons. The dielectric response of each subshell is calculated separately, including in this way the screening among the electrons of the same binding energy. Results for stopping and straggling cross sections of protons in Au, Pb, and Bi are compared with the available experimental data. The theoretical stopping results are very good in the case of Au, reproducing the experimental data in an extensive energy region (10 keV–100 MeV). For Pb and Bi, the stopping results agree with the measurements for energies above 300 keV, for which the inner shells play a major role. However, we found some difficulties around the stopping maximum. For the energy-loss straggling, we obtained reasonably good agreement with the experiments for the three targets studied.

DOI: 10.1103/PhysRevA.79.032903 PACS number(s): 34.50.Bw

I. INTRODUCTION

The stopping power of ions is a necessary ingredient of many parts of basic science, of medical and technological applications [1,2]. It is an average of the ion energy loss per unit path length. At intermediate to high impact velocities, this energy loss is related to excitation or ionization of target electrons. The higher the ion energy, the deeper the excited electrons. In the case of metals, it means that at intermediate and high impact energies, the description of the stopping power due to excitation of the free-electron gas (FEG) is not enough, and target bound electrons must be included.

Different experimental methods are used to determine stopping powers [3] and important collections of data and statistics of the results are available in the web [4,5]. Many semiempirical [6–9] and theoretical models [10–15] have been developed. However, the description of very heavy targets, i.e., those with the close $4f$ shell with its 14 electrons, remains a heavy task for *ab initio* theoretical calculations.

In the last years we have explored the possibilities and ranges of validity of the shellwise local plasma approximation (SLPA) [16–18]. This is a many-electron model especially suitable for multielectronic targets. The SLPA is based on Lindhard and Scharff's seminal work [19], the local plasma approximation (LPA), which has been widely used and improved since then [20,21], mainly with the fully dielectric formulation [22–24], instead of the logarithmic high-energy limit.

In the LPA the response of bound electrons, even local, considers the electronic cloud as a whole by using the total density of electrons. The SLPA introduces two main changes to this approach: a separate dielectric response for each shell and the explicit inclusion of the ionization thresholds using the Levine and Louie [25] dielectric function. Physically, this independent shell approximation means that when an electron of the nl-subshell is ionized only the other nl-electrons are included in the screening of the ion potential. A previous proposal of independent shells within de LPA is the orbital LPA by Meltzer *et al.* [26]; however this approach uses the logarithmic high-energy limit for the stopping power.

The wave functions and binding energies of target electrons are the only input for the SLPA. So far, we have employed this model with good results [16–18] for elements with atomic number $Z_T \leq 54$, using the well-known Hartree-Fock wave functions for neutral atoms reported by Bunge [27] or Clementi-Roetti [28].

The aim of this work is to present and discuss theoretical calculations of energy loss and energy-loss straggling for protons in targets with atomic number $Z_T > 54$. The description of these atoms requires the solution of the relativistic Dirac equation instead the nonrelativistic Schrödinger equation. To this end we made fully relativistic *ab initio* calculations by employing the HULLAC [29,30] and the GRASP [31,32] computer packages. These two codes evolved and have been widely used over the years, representing the *state-of-the-art* in atomic structure calculations.

This fully relativistic study allows us to extend the field of application of the SLPA to heavier atoms. On the other hand, this many-electron model is especially suitable for the description of shells such as the $4f$, for which the shielding effects are expected to be important.

We present here total stopping and straggling cross sections for protons in Pb, Bi, and Au. In the case of Pb and Bi, in spite of their technological and medical applications [33,34], the stopping cross sections are not well defined experimentally, especially around the stopping maximum. On the other hand, to our knowledge, no previous *ab initio* calculations have been developed for these systems. The case of Au is just the opposite. It has been extensively studied, being the element with the greatest number of stopping measurements (66 groups of data [4] since those by Bätzner in 1936

*mclaudia@iafe.uba.ar

[35]). This makes Au a good benchmark for any theoretical description.

We describe the theoretical formulation in Sec. II. In Sec. III, our results are compared with the experimental data available [4,5], with the semiempirical SRIM 2008 values [5] and, in the case of Gold, with recent theoretical results by Heredia-Avalos *et al.* [36].

II. THEORETICAL CALCULATIONS

A. Densities and binding energies

We have explored two set of semirelativistic wave functions generated by the AUTOSTRUCTURE code [37–39] and two fully relativistic calculations obtained with the HULLAC [29,30] and the GRASP [31,32] computer packages. Details are presented next. We anticipate that, for the present stopping and straggling calculations, the GRASP results were employed because they provide the most reliable description of the binding energies as compared with experimental data. Nevertheless the difference using the HULLAC or the GRASP results was found to be less than 5% in the total stopping and negligible in the energy-loss straggling.

1. Semirelativistic method

The AUTOSTRUCTURE code [37–39] is used to calculate multiconfiguration intermediate coupling energy levels. The code can make use both of nonrelativistic and semirelativistic wave functions [40]. It represents the core of the atomic data and analysis structure (ADAS) set [41] for modeling the radiating properties of ions and atoms for plasmas ranging from the interstellar medium through the solar atmosphere and laboratory thermonuclear fusion devices to technological plasmas (see [42], for example).

In order to keep the problem of calculating energy levels and spectra as simple as possible, it is worthwhile seeking some approximate method of incorporating the major relativistic effects within the format of the nonrelativistic approach. The AUTOSTRUCTURE code generates the semirelativistic bound orbital functions, following the work of Cowan and Griffin [43]. Within this approach, the mass velocity and Darwin terms of the Pauli equation for one-electron atoms have been added to the usual nonrelativistic one-electron Hartree-Fock differential equations. Perturbation theory is used to evaluate the remaining one-body (namely, nuclear spin- orbit) and two-body fine-structure interactions (spin-orbit, spin-other-orbit and spin-spin) and two-body non-fine-structure interactions (i.e., contact spin-spin two-body Darwin and orbit-orbit operators).

The code also allows us to generate two set of semirelativistic wave funcions. In the first set, the core radial functions were determined using an *N*-electron Thomas-Fermi-Dirac-Amaldi (TFDA) model potential. In the second set, radial wave functions are calculated in Hartree potential evaluated with Slater-type orbital (STO) functions. In both cases, the orbitals are Schmidt orthogonalized. All the calculations have been produced in intermediate coupling approximation.

2. Relativistic approach

Two different sets of fully relativistic calculations for the atomic structure were performed by using the HULLAC [29,30] and the GRASP [31,32] codes.

The HULLAC code [29,30] is used in structure and cross-section calculations for collisional and radiative atomic processes. The theoretical framework of this code is the first-order perturbation theory with a central field. The zero-order wave functions are solutions of the Dirac equation. The Hamiltonian is diagonalized on the basis of these wave functions (configuration interaction). The first-order perturbation theory contribution from the Breit interaction energies is also included in the calculations, as well as quantum electrodynamics corrections. In this package, the detailed level energies are calculated using the fully relativistic multiconfigurational RELAC code [44], based on the parametric potential model [45]. The main idea of the parametric potential method is to describe simply the screening of some sensible parametrized charge distribution. This is done by the introduction of a central potential as an analytic function of screening parameters which are determined by minimizing the first-order relativistic energy of a set of configurations. This optimized potential is used to calculate all one-electron orbitals and energies, relativistic multiconfiguration bound states and their energies, continuum orbitals, and all the required transition rates. This code is focused on heavy ionized atoms with several open shells but can be applied to other atomic systems, as in the present work.

The GRASP code, developed by Grant *et al.* [31,32] is based on the multiconfiguration Dirac-Hartree-Fock (MCDHF) method. It is a fully relativistic code, based on the *jj* scheme, which includes also Breit interactions and QED effects. The MCDHF equations are derived by using the variational approach on an energy functional, defined as a linear combination of energy eigenvalues. In the variational part of the calculations, the Dirac-Coulomb Hamiltonian is written as

$$\hat{H}_{DC} = \sum_i \left(\alpha_i \dot{p}_i c + \beta_i c^2 - \frac{Z}{r_i} \right) + \sum_{i \neq j} \frac{1}{r_{ij}}. \quad (1)$$

The binding energies are a very sensitive parameter of the method employed. In Fig. 1 we display the atomic binding energies of Au, Pb, and Bi obtained with the four different methods, the semirelativistic using the AUTOSTRUCTURE code, in STO and TFDA, and the fully relativistic GRASP and HULLAC codes. Semirelativistic results have no spin-orbit split in energy $E_{n,l,l\pm 1/2}$ (hereafter $nl\pm$), so we plot each value twice, the same for both levels, just to make the comparison easier. As Fig. 1 shows, we found an important difference between STO results and the TFDA or both fully relativistic calculations. The relative difference increases for the outer shells, but in absolute value this effect appears even for the *K* shell. The semirelativistic TFDA energies are in good agreement with the fully relativistic ones, except for the 4*f* shells which are systematically deeper bound than the 5*s* shells in the three elements, as can be observed in Fig. 1.

Figure 1 also includes the experimental data for the binding energies in solids compiled by Williams [46]. Those

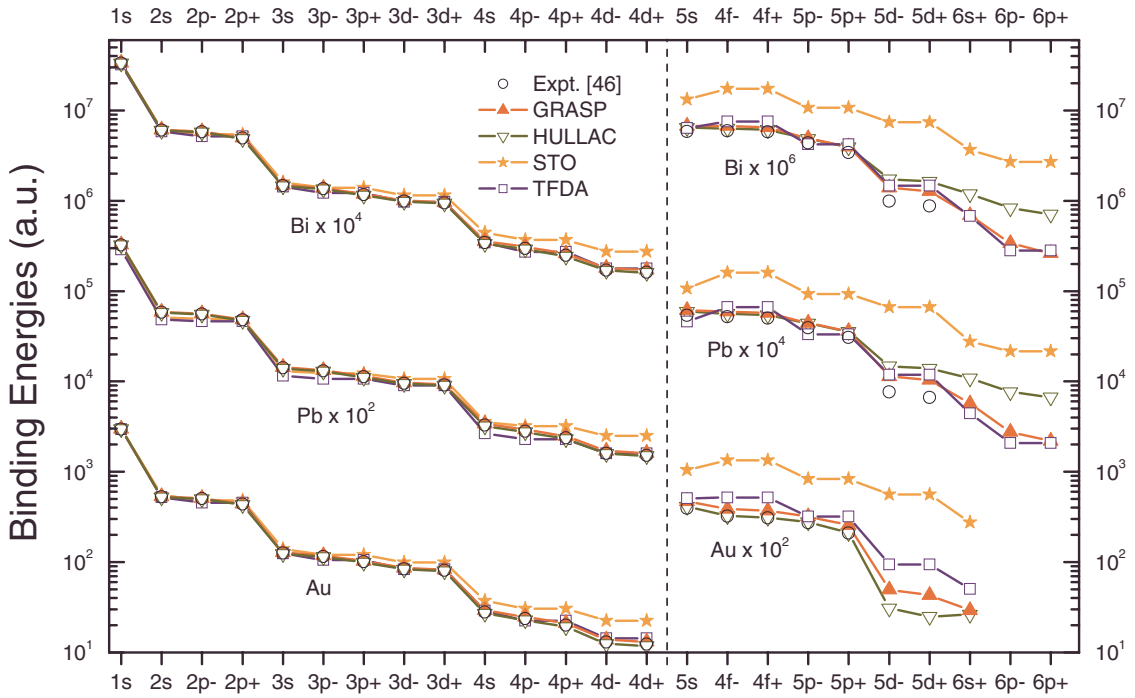

FIG. 1. (Color online) Electronic binding energies of Au, Pb, and Bi. Symbols: stars, semirelativistic STO; hollow squares, semirelativistic TFDA; up-filled triangles, relativistic GRASP; down hollow triangles, relativistic HULLAC; hollow circles, experimental data in solids [46].

shells whose electrons are part of the solid FEG can be distinguished because no experimental binding energies are plotted. The gas-solid difference is found only in the outer shells, as expected. The GRASP and HULLAC results are in very good agreement with the experimental binding energies. We found an important experimental-theoretical difference only for the $5d$ subshell of Pb and Bi. In these cases the GRASP results provide more reliable values as compared with experimental data. On this basis, we employed the GRASP results for the energy-loss and straggling calculations. It is worth mentioning that the comparison of both fully relativistic methods showed the difference in total stopping cross sections to be less than 5%, and in the energy-loss straggling less than 1%.

B. Stopping and straggling calculations

The energy loss by the impinging ion due to ionization of target bound electrons is calculated by employing the SLPA [16–18]. As mentioned before, the electronic density of each shell and its binding energy are the only inputs. If they are available, the SLPA calculation let us to describe any target with the same degree of complexity. Furthermore, the more electrons the shell has, the more suitable the method is. On the other hand, this model works within the dielectric formalism, so dynamic screening effects among electrons belonging to the same shell are included. This is of particular interest for the case of the f shells treated in this work.

Within the SLPA, the energy moment of order t ($t=0$ cross section, $t=1$ stopping, and $t=2$ square of the straggling) associated with the ionization of at least one electron of the nl subshell due to the interaction with an ion of impact velocity v is expressed as [18]

$$S_{nl}^{t}(v) = \frac{2Z_P^2}{\pi v^2}\int_0^\infty \frac{dk}{k}\int_0^{kv} \omega^t \,\mathrm{Im}\left[\frac{-1}{\varepsilon_{nl}(k,\omega)}\right]d\omega, \qquad (2)$$

where

$$\mathrm{Im}\left[\frac{-1}{\varepsilon_{nl}(k,\omega)}\right] = 4\pi\int_0^{R_{WS}} \mathrm{Im}\left[\frac{-1}{\varepsilon(k,\omega,\delta_{nl}(r),E_{nl})}\right]r^2 dr. \qquad (3)$$

Equation (2) is the usual expression in the dielectric formalism. Equation (3) is the space mean-value over the atomic dimensions [$(\frac{4}{3}\pi R_{WS}^3)^{-1}=\delta_{at}$, the atomic density] for an inhomogeneous gas of electrons of density $\delta_{nl}(r)$ and ionization gap E_{nl}. The dielectric function employed is the Levine-Louie one [25], which includes explicitly the energy gap of each shell [17,18]. It keeps up the characteristics of Lindhard dielectric function [47], such as linear response and electron-electron correlation to all orders, and satisfies the f-sum rule (particle number conservation).

In this work the densities and binding energies are obtained from the fully relativistic wave functions described in the previous subsection. Total stopping or square straggling are calculated adding the independent shell contributions.

We considered together those electrons of the same binding energy $E_i \pm \Delta E_i$, with ΔE_i being the quantum uncertainty

TABLE I. FEG parameters for Au, Pb, and Bi from their optical data of energy-loss function [52–54]: Ne, number of electrons; r_S, Seitz radius; ω_p, plasma frequency; and γ, width. All of them in atomic units.

Element	Ne	r_S	ω_p	γ
Au	17.0	1.17	1.37	1.37
Pb	3.7	2.37	0.47	0.15
Bi	5.6	2.17	0.54	0.28

$$\Delta E_i \geq \frac{\hbar}{\Delta t} = \frac{\hbar v}{\langle x \rangle_i}$$

and $\langle x \rangle_i$ being the mean radius of the shell. If the spin-orbit split between $nl+$ and $nl-$ is less than the quantum uncertainty in energy, the electrons are considered to react together shielding the projectile; i.e., the 14 electrons of the $4f$ subshell as a whole and not the 8 electrons $4f+$ and the 6 electrons $4f-$ separately. In all cases the screening among electrons reduces the stopping cross section. In the three cases studied (Au, Pb, and Bi), this reduction due to screening between $nl\pm$ shells was found to be appreciable for energies above the stopping maximum (i.e., 5%–10% in the energy range 0.2–3 MeV) and tends to be negligible for very high energies (above 4 MeV).

Different works about the binding energies of H ions inside an electron gas consider that, at low velocities, the screening of the H^+ nucleus is strong enough to have very loose or directly no bound electron [48–50]. In what follows we calculate stopping and straggling in multielectronic targets just considering H^+.

III. RESULTS

In order to compare with the experimental data available we present total results for the stopping and square straggling cross sections. To this end we have added the contribution of the FEG to that of bound electrons calculated with the SLPA. It was done within the perturbative approximation using the Mermin dielectric function [51]. The characteristic plasmon frequencies ω_p and widths γ of the FEG were obtained from the optical data of Au [52], Pb [53], and Bi [54], considering the first important peak in the energy-loss function. These values were also tested with another tabulation of experimental plasmon frequencies by Isaacson [55]. The values employed in this work are displayed in Table I.

The perturbative calculation for the FEG using Mermin dielectric function [51] is expected to describe the experimental data for energies above 50 keV. Nonperturbative results for the FEG contribution can be added to the present SLPA to have a better description at low energies.

A. Gold

The atomic binding energies of Au were included in Fig. 1. For solid Au, the atomic $5p^6$, $5d^{10}$, and $6s^1$ electrons were considered as the homogeneous FEG (see the values in Table I), so the first shell of bound electrons is the $4f$ subshell with its 14 electrons (the $5s$ is the second one).

In Fig. 2 we display our theoretical results for the stopping cross section together with the large amount of experimental data available [4] and the SRIM 2008 values [5]. We also include in this figure the theoretical curve by Heredia-Avalos *et al.* [36].

Our total stopping cross section describes the data quite well in the whole energy range. There is an important dispersion of experimental values, mainly around the stopping maximum. In order to analyze the results, we have classified the data chronologically. Only the stopping measurements of the last 20 years [56–64] are displayed separately in the figure. This arbitrary classification allowed us to note that, except for the results by Martinez-Tamayo *et al.* [56], the latest stopping measurement tend to be close to a single curve. The semiempirical SRIM 2008 code [5] gives a curve in accordance with these latest experimental data.

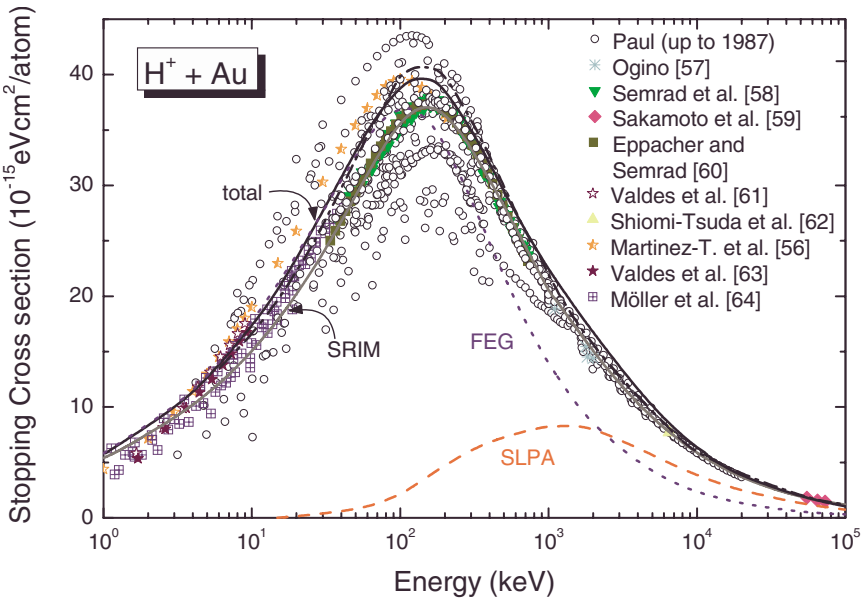

FIG. 2. (Color online) Stopping cross section of Au for protons. Curves: dashed-line, present SLPA calculation for the bound electrons; dotted-line, FEG contribution using the Mermin dielectric function [51]; black solid line, total stopping as the addition of the previous two contributions; gray solid line, SRIM 2008 [5]; dashed-dotted line, recent theoretical calculation by Heredia-Avalos *et al.* [36]. Symbols: experimental data [4,56–64] as indicated in the figure.

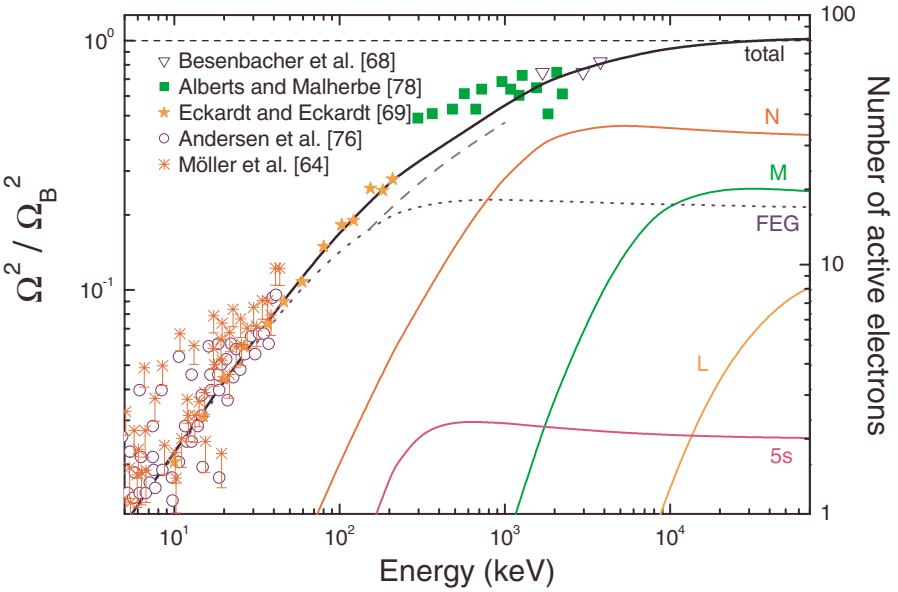

FIG. 3. (Color online) Squared straggling of Au for protons normalized to Bohr high-energy limit. Curves: solid-lines, our SLPA results for the different shells of bound electrons; dotted line, contribution of the FEG using the Mermin dielectric function [51]; dashed line, total LPA results by Chu [67]. Symbols: experimental data [68,69,76–78] as indicated in the figure.

The contributions of the FEG and the bound electrons are displayed separately in Fig. 2. The FEG contribution in gold is the main one but cannot explain the total results for energies above 100 keV.

The total stopping cross section shows a maximum at 130 keV, shifted with respect to SRIM, and in rather good agreement with the measurements by Martinez-Tamayo *et al.* [56], and to previous ones by Kreussler *et al.* [65] and Santry and Werner [66]. Very similar theoretical results were obtained in Ref. [36].

The square energy-loss straggling of protons in Au is displayed in Fig. 3, which fits the experimental data very well. We also include in this figure the theoretical results by Chu [67] using the LPA with Hartree-Fock densities but considering the electronic density as a whole. The difference between our results and those by Chu is due to the independent shell approximation considered in the present SLPA.

The theoretical square energy-loss straggling, calculated as the second moment of the energy by Eq. (2), describes only the statistical straggling. However, the measured straggling includes the contribution due to surface roughness and inhomogeneity in the foil thickness [68–75]. Some straggling measurements are corrected by subtracting this contribution from the experimental measurements. Instead, other publications add this contribution to the statistical calculations [76,77]. In Fig. 3 we have included only those experimental sets of data that explicitly take into account the roughness and inhomogenity of the sample. In the case of the experimental data by Andersen *et al.* [76], they have been corrected in 10% due to the estimation of this contribution in Ref. [76]. The data by Möller *et al.* [77] shows asymmetric error bars that correspond to Fig. 5 in Ref. [77].

The theoretical square straggling plotted in Fig. 3 is normalized to the Bohr high-energy limit [79]. The total values displayed are calculated as the addition of the FEG and the different shells contributions. In Fig. 3 we add the *nl* subshells just for simplicity and show the total *L*, *M*, and *N* shells. It is interesting to note that the total square straggling tends to the Bohr limit—proportional to the total number of electrons in the target, all active in the high-energy collision. In the same way, at high energies the contribution of the FEG and every shell tends to the number of electrons in them. To stress this point, we scaled the right axis as the number of active electrons $N(v)=Z_T\ \Omega^2(v)/\Omega_B^2$. At certain energy all the electrons of the subshell are active and the contribution to the straggling saturates to almost a constant.

The total straggling tends to Bohr from below and do not show the overshooting around the energy of maximum stopping power predicted by the binary collision formalisms [80,81]. Nevertheless, we note that each shell contribution grows with increasing proton velocity, reaching values above the saturation limit at certain energies. This effect does not appear in the total straggling.

B. Lead

In Fig. 4 we display our theoretical results for the total stopping cross section of protons in Pb, showing also the partial contributions from the FEG and from the bound shells. In this case the contribution of bound electrons plays a major role. The comparison with the experimental data available shows good agreement for energies above 300 keV (overestimation of 7% at 2 MeV with respect to the data by Ogino [57]). In this high-energy region the different experimental data agree nicely, but near the stopping maximum the data by Bader *et al.* [82], measured in 1956, differs in about 10% from the more recent data by Eppacher and Semrad [60] or Sirotonin [83]. Note that the SRIM results [5] follow the maximum measured by Bader *et al.* [82]. Our theoretical results have an undesirable two-peak shape around the stopping maximum; however it is 5% above and below the data by Eppacher and Semrad [60].

A nonperturbative description of the FEG contribution could be very useful in this case. The high Seitz radius of lead (r_s=2.30 a.u.) suggests an important difference between the non-perturbative and the linear response calculations for the FEG [90]. In the low energy, the lack of experimental data below 30 keV leaves the description of the stopping of protons in lead still open.

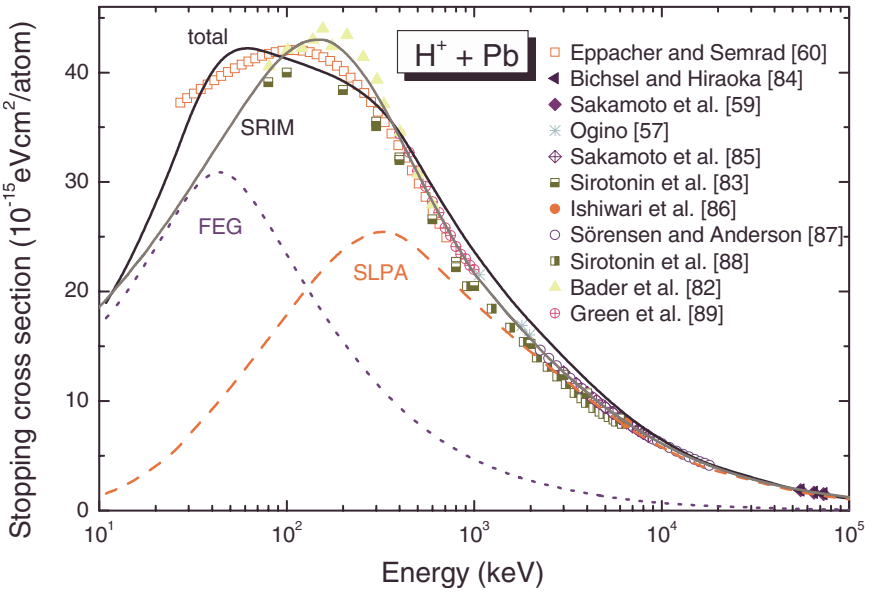

FIG. 4. (Color online) Stopping power of Pb for protons. Curves: as in Fig. 2. Symbols: experimental data [57,59,60,82–89] as indicated in the figure.

The energy-loss straggling for protons in Pb is displayed in Fig. 5. The general behavior of the theoretical results is the same as that obtained in Fig. 3 for Au. Again we plotted separately the contributions of the FEG and the different bound shells. Only one set of experimental data, by Malherbe and Alberts [91], was found for this system, and the theoretical-experimental agreement is reasonable, at least above 800 keV.

C. Bismuth

The theoretical results for stopping of protons in Bi are displayed in Fig. 6. As can be observed, they tend to describe the experimental data for energies above 300 keV (with an overestimation of 10% at 2 MeV with respect to Ogino measurements [57]). Our calculations in Bi show the same difficulty around the maximum as in the case of Pb. Again, we have the two-peak shape following the FEG and SLPA curves. On the other hand, our results are near the latest measurements of stopping in Bi by Eppacher [92]. This data has a maximum at the same energy (100 keV) but 15% below the data by Krist and Mertens [93] or Eckardt [94] and the SRIM curve. It would be desirable to have new measurements in this energy region (30–400 keV).

In Fig. 7 we compare our theoretical straggling with the experimental measurements by Eckardt [94], with very good agreement in the whole energy range. We also include more recent measurements by Eckardt and Lantschner [69] but only at 200 keV. As in the case of gold, we include in this figure the theoretical results by Chu [67] using the LPA with all the shells together. As expected, this curve is always below the SLPA.

In the three cases studied (Au, Pb, and Bi) we reproduce Bethe high-energy limit for the stopping power within 2% for impact energies above 3 MeV. However, a systematic overestimation of the experimental data in about 5% is found for energies of a few MeVs. This indicates that perhaps more complex mechanisms not included in our calculation should be considered.

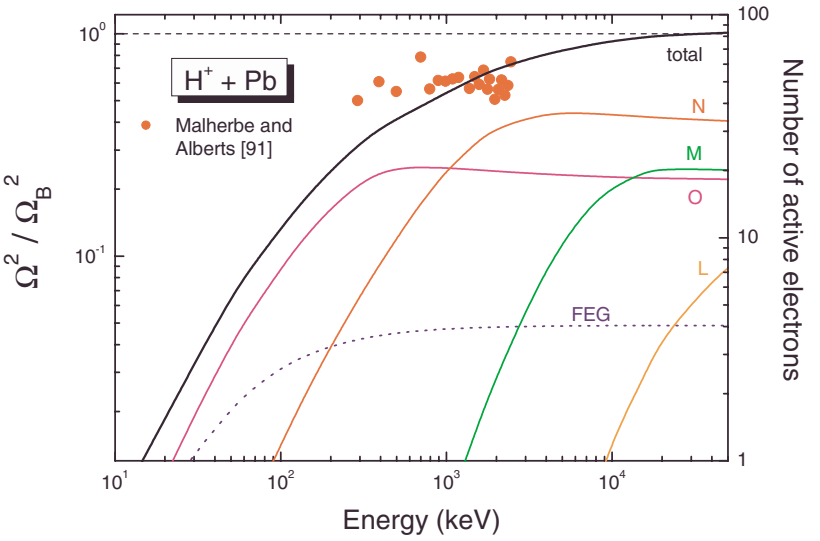

FIG. 5. (Color online) Normalized squared straggling of Pb for protons. Curves: as in Fig. 3. Symbols: experimental data by Malherbe *et al.* [91]

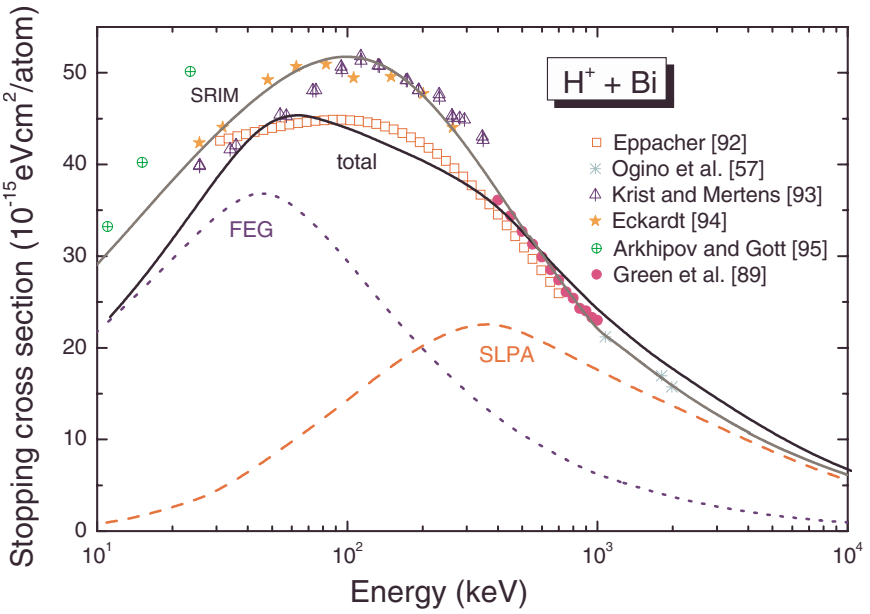

FIG. 6. (Color online) Stopping power of Bi for protons. Curves: as in Fig. 2. Symbols: experimental data [57,89,92–95] as indicated in the figure.

IV. CONCLUDING REMARKS

We present in this work *ab initio* calculations of stopping and energy-loss straggling cross sections of protons in Au, Pb, and Bi. We employed the dielectric formalism and linear response for the FEG and the SLPA for the inner shells. The SLPA considers the local free-electron-gas approximation of the LPA, but within the independent shell approximation for the electronic response, and the Levine and Louie dielectric function including the ionization threshold of each shell. Fully relativistic electronic densities and binding energies were calculated numerically by employing the HULLAC and the GRASP codes and are compared with experimental binding energies in solids with very good agreement.

The theoretical stopping values are very good in the case of gold even at lower energies than the expected ones for a perturbative method. For lead and bismuth, the stopping results are good for energies above 300 keV, for which the inner shells play a major role. However, we found some difficulties around the stopping maximum. An overestimation of the experimental data in about 5% is found for energies of a few MeVs, indicating the presence of mechanisms not included in this formalism. Our straggling results describe the experimental data in the three cases reasonably well, approaching the Bohr high-energy limit from below.

We want to stress that we have dealt with multielectronic targets (with 79 up to 83 bound electrons). These atoms have the complete $4f$ subshell as one of the outer ones, playing an important role in the stopping calculations. The SLPA does not use any external parameter, but the fully theoretical densities and binding energies. We think that the SLPA can be considered as a reliable approximation to treat very heavy elements.

ACKNOWLEDGMENTS

The authors acknowledge N. R. Arista for his useful com-

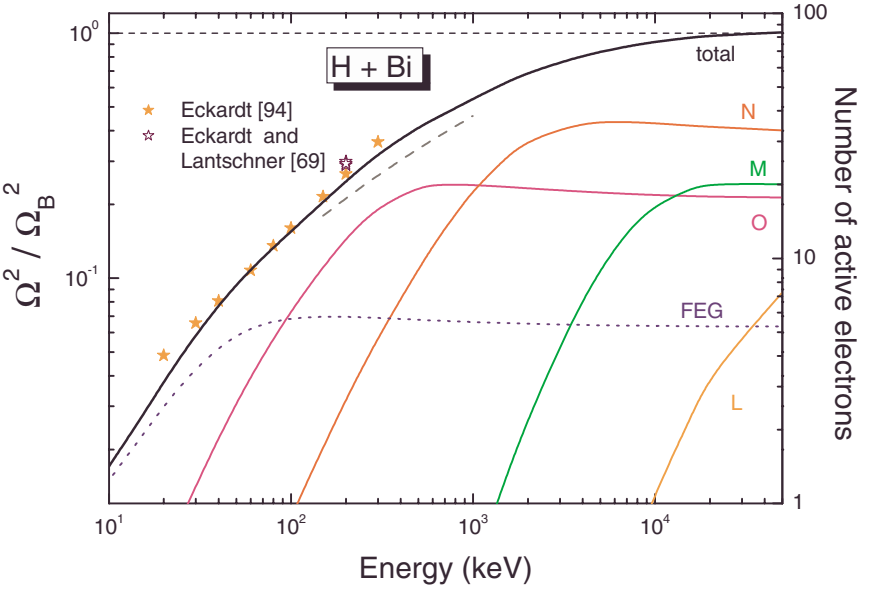

FIG. 7. (Color online) Normalized squared straggling of Bi for protons. Curves: as in Fig. 3. Symbols: experimental data [69,94] as indicated in the figure.

ments about this work and J. Garcia de Abajo for suggestions about the energy-loss function. We also appreciate illuminating clarifications about stopping and straggling experimental measurements by J. C. Eckardt and G. H. Lantschner. This work was partially supported by the Universidad de Buenos Aires, the Agencia Nacional de Promoción Científica y Tecnológica of Argentina, the Consejo Nacional de Investigaciones Científicas y Técnicas (CONICET).

[1] H. Paul, Nucl. Instrum. Methods Phys. Res. B **261**, 1176 (2007).
[2] International Commission on Radiation Units and Measurements, Bethesda, MD, ICRU Report No. 73 (Oxford Univ. Press, Oxford, 2005).
[3] International Commission on Radiation Units and Measurements, Bethesda, MD, ICRU Report No. 49 (Bethesda, MD, 1993).
[4] H. Paul, *Stopping Power for Light Ions: Graphs, Data, Comments and Programs* in http://www.exphys.uni-linz.ac.at/stopping/
[5] J. F. Ziegler, http://www.srim.org
[6] H. Paul and A. Schinner, At. Data Nucl. Data Tables **85**, 377 (2003).
[7] H. H. Andersen and J. F. Ziegler, *Hydrogen Stopping Powers and Ranges in All Elements* (Pergamon, New York, 1977).
[8] J. F. Ziegler, J. P. Biersack, and M. D. Ziegler, *SRIM The Stopping and Range of Ions in Matter* (SRIM Co., Chester, MD, 2008).
[9] F. Hubert, R. Bimbot, and H. Gauvin, At. Data Nucl. Data Tables **46**, 1 (1990).
[10] P. L. Grande and G. Schiwietz, in *Advances in Quantum Chemistry*, edited by J. Sabin (Elsevier, New York, 2004), Vol. 45, p. 7.
[11] N. R. Arista and A. F. Lifschitz, in *Advances in Quantum Chemistry*, edited by J. Sabin (Elsevier, 2004), Vol. 45, p. 47.
[12] P. Sigmund and A. Schinner, Nucl. Instrum. Methods Phys. Res. B **195**, 64 (2002).
[13] S. Heredia-Avalos, J. C. Moreno-Marin, I. Abril, and R. Garcia-Molina, Nucl. Instrum. Methods Phys. Res. B **230**, 118 (2005).
[14] C. C. Montanari and J. E. Miraglia, Phys. Rev. A **73**, 024901 (2006).
[15] G. Maynard, M. Sarrazin, K. Katsonis, and K. Dimitriou, Nucl. Instrum. Methods Phys. Res. B **193**, 20 (2002).
[16] A. J. Garcia and J. E. Miraglia, Phys. Rev. A **74**, 012902 (2006).
[17] C. D. Archubi, C. C. Montanari, and J. E. Miraglia, J. Phys. B **40**, 943 (2007).
[18] C. C. Montanari, J. E. Miraglia, M. Behar, P. F. Duarte, N. R. Arista, J. C. Eckardt, and G. H. Lantschner, Phys. Rev. A **77**, 042901 (2008).
[19] J. Lindhard and M. Scharff, Mat. Fys. Medd. K. Dan. Vidensk. Selsk. **27**, 1 (1953).
[20] E. Bonderup, Mat. Fys. Medd. K. Dan. Vidensk. Selsk. **35**, 17 (1967).
[21] W. K. Chu and D. Powers, Phys. Lett. A **40**, 23 (1972).
[22] C. M. Kwei, T. L. Lin, and C. J. Tung, J. Phys. B **21**, 2901 (1988).
[23] Y. N. Wang and T. C. Ma, Phys. Rev. A **50**, 3192 (1994).
[24] J. D. Fuhr, V. H. Ponce, F. J. García de Abajo, and P. M. Echenique, Phys. Rev. B **57**, 9329 (1998).
[25] Z. H. Levine and S. G. Louie, Phys. Rev. B **25**, 6310 (1982).
[26] D. E. Meltzer, J. R. Sabin, and S. B. Trickey, Phys. Rev. A **41**, 220 (1990).
[27] C. F. Bunge, J. A. Barrientos, A. V. Bunge, and J. A. Cogordan, Phys. Rev. A **46**, 3691 (1992).
[28] E. Clementi and C. Roetti, At. Data Nucl. Data Tables **14**, 177 (1974).
[29] J. Oreg, W. H. Goldstein, M. Klapisch, and A. Bar-Shalom, Phys. Rev. A **44**, 1750 (1991).
[30] A. Bar-Shalom, M. Klapisch, and J. Oreg, J. Quant. Spectrosc. Radiat. Transf. **71**, 169 (2001).
[31] I. P. Grant, B. J. McKenzie, P. H. Norrington, D. F. Mayers, and N. C. Pyper, Comput. Phys. Commun. **21**, 207 (1980).
[32] B. J. McKenzie, I. P. Grant, B. J. McKenzie, and P. H. Norrington, Comput. Phys. Commun. **21**, 233 (1980).
[33] J. Sweezy, N. Hertel, and A. Lennox, Radiat. Prot. Dosim. **116**, 470 (2005).
[34] K. Kin'Ya, K. Teruaki, and O. Mikinori, Mitsui Zos. Tech. Rev. **182**, 14 (2004).
[35] H. Bätzner, Ann. Phys. **25**, 233 (1936).
[36] S. Heredia-Avalos, I. Abril, C. D. Denton, J. C. Moreno-Marín, and R. Garcia-Molina, J. Phys.: Condens. Matter **19**, 466205 (2007).
[37] N. R. Badnell, J. Phys. B **19**, 3827 (1986).
[38] N. R. Badnell and M. S. Pindzola, Phys. Rev. A **39**, 1685 (1989).
[39] N. R. Badnell, J. Phys. B **30**, 1 (1997).
[40] M. S. Pindzola and N. R. Badnell, Phys. Rev. A **42**, 6526 (1990).
[41] See, for example, the ADAS Manual at http://adas.phys.strath.ac.uk/manual.php
[42] N. R. Badnell, M. G. O'Mullane, H. P. Summers, Z. Altun, M. A. Bautista, J. Colgan, T. W. Gorczyca, D. M. Mitnik, M. S. Pindzola, and O. Zatsarinny, Astron. Astrophys. **406**, 1151 (2003).
[43] R. D. Cowan and D. C. Griffin, J. Opt. Soc. Am. **66**, 1010 (1976).
[44] M. Klapisch, J. L. Schwob, B. S. Frankel, and J. Oreg, J. Opt. Soc. Am. **67**, 148 (1977).
[45] M. Klapisch, Comput. Phys. Commun. **2**, 239 (1971).
[46] G. P. Williams, *Electron Binding Energies of the Elements*, CRC Handbook of Chemistry and Physics 66th Edition Vol. F170 (CRC Press, Boca Raton, 1986).; G. P. Williams, *Electron Binding Energies*, X-Ray Data Booklet (Lawrence Berkeley Laboratory, Berkeley, CA, 1986) Chap. 2.2; or in the web, an updated version can be found at http://www.jlab.org/ gwyn/ebindene.html
[47] J. Lindhard, Mat. Fys. Medd. K. Dan. Vidensk. Selsk. **28**, 8 (1954).
[48] N. R. Arista,Mat. Fys. Medd. K. Dan. Vidensk. Selsk. **52**, 595

(2006).
[49] T. L. Ferrell and R. H. Ritchie, Phys. Rev. B **16**, 115 (1977).
[50] J. Müller and J. Bürgdorfer, Phys. Rev. A **43**, 6027 (1991).
[51] N. D. Mermin, Phys. Rev. B **1**, 2362 (1970).
[52] *The Electronic Handbook of Optical Constants of Solids*, edited by E. D. Palik and G. Ghosh (Academic, San Diego, CA, 1999).
[53] A. M. Ashton and G. W. Green, J. Phys. F: Met. Phys. **3**, 179 (1973).
[54] C. Wehenkel and B. Gauthe, Solid State Commun. **15**, 555 (1974).
[55] D. Isaacson, *New York University, Doc. No. 02698* (National Auxiliary, New York, 1975).
[56] G. Martinez-Tamayo, J. C. Eckardt, G. H. Lantschner, and N. R. Arista, Phys. Rev. A **54**, 3131 (1996).
[57] K. Ogino, T. Kiyosawa, and T. Kiuchi, Nucl. Instrum. Methods Phys. Res. B **33**, 155 (1988).
[58] D. Semrad, C. Eppacher, and R. Tober, Nucl. Instrum. Methods Phys. Res. B **48**, 79 (1990).
[59] N. Sakamoto, H. Ogawa, M. Mannami, K. Kimura, Y. Susuki, M. Hasegawa, I. Hatayama, T. Noro, and H. Ikegami, Radiat. Eff. Defects Solids **117**, 193 (1991).
[60] Ch. Eppacher and D. Semrad, Nucl. Instrum. Methods Phys. Res. B **69**, 33 (1992).
[61] J. E. Valdes, G. Martinez-Tamayo, G. H. Lantschner, J. C. Eckardt, and N. R. Arista, Nucl. Instrum. Methods Phys. Res. B **73**, 313 (1993).
[62] N. Shiomi-Tsuda, N. Sakamoto, and R. Ishiwari, Nucl. Instrum. Methods Phys. Res. B **93**, 391 (1994).
[63] J. E. Valdes, C. Agurto, F. Ortega, P. Vargas, R. Labbé, and N. R. Arista, Nucl. Instrum. Methods Phys. Res. B **164-165**, 268 (2000).
[64] S. P. Möller, A. Csete, T. Ichioka, H. Knudsen, U. I. Uggerhoj, and H. H. Andersen, Phys. Rev. Lett. **88**, 193201 (2002).
[65] S. Kreussler, C. Varelas, and R. Sizmann, Phys. Rev. B **26**, 6099 (1982).
[66] D. C. Santry and R. D. Werner, Nucl. Instrum. Methods Phys. Res. **188**, 211 (1981).
[67] W. K. Chu, Phys. Rev. A **13**, 2057 (1976).
[68] F. Besenbacher, J. U. Andersen, and E. Bonderup, Nucl. Instrum. Methods **168**, 1 (1980).
[69] J. C. Eckardt and G. H. Lantschner, Nucl. Instrum. Methods Phys. Res. B **175-177**, 93 (2001); G. Lantschner, private communication (2008).
[70] Y. Kido, Phys. Rev. B **34**, 73 (1986); Nucl. Instrum. Methods Phys. Res. B **24-25**, 347 (1987).
[71] Y. Kido and T. Koshikawa, Phys. Rev. A **44**, 1759 (1991).
[72] J. C. Eckardt and G. H. Lantschner, Thin Solid Films **249**, 11 (1994).
[73] D. W. Moon, H. I. Le, K. J. Kim, T. Nishimura, and Y. Kido, Nucl. Instrum. Methods Phys. Res. B **183**, 10 (2001).
[74] D. G. Arbó, M. S. Gravielle, J. E. Miraglia, J. C. Eckardt, G. H. Lantschner, M. Famá, and N. R. Arista, Phys. Rev. A **65**, 042901 (2002).
[75] M. Tosaki, J. Appl. Phys. **99**, 034905 (2006).
[76] H. H. Andersen *et al.*, Nucl. Instrum. Methods Phys. Res. B **194**, 217 (2002).
[77] S. P. Möller *et al.*, Eur. Phys. J. D **46**, 89 (2008).
[78] H. W. Alberts and J. B. Malherbe, Radiat. Eff. **69**, 231 (1983).
[79] N. Bohr, Philos. Mag. **30**, 581 (1915).
[80] M. S. Livingston and H. A. Bethe, Rev. Mod. Phys. **9**, 245 (1937).
[81] P. Sigmund and A. Schinner, Eur. Phys. J. D **23**, 201 (2003).
[82] M. Bader, R. E. Pixley, F. S. Mozer, and W. Whaling, Phys. Rev. **103**, 32 (1956).
[83] E. I. Sirotinin, A. F. Tulinov, V. A. Khodyrev, and V. N. Mizgulin, Nucl. Instrum. Methods Phys. Res. B **4**, 337 (1984).
[84] H. Bichsel and T. Hiraoka, Nucl. Instrum. Methods Phys. Res. B **66**, 345 (1992).
[85] N. Sakamoto, N. Shiomi, H. Ogawa, and R. Ishiwari, Nucl. Instrum. Methods Phys. Res. B **13**, 115 (1986).
[86] R. Ishiwari, N. Shiomi-Tsuda, and N. Sakamoto, Nucl. Instrum. Methods Phys. Res. B **2**, 141 (1984).
[87] H. Sörensen and H. H. Andersen, Phys. Rev. B **8**, 1854 (1973).
[88] E. I. Sirotinin, A. F. Tulinov, A. Fiderkevich, and K. S. Shyshkin, Radiat. Eff. **15**, 149 (1972).
[89] D. W. Green, J. N. Cooper, and J. C. Harris, Phys. Rev. **98**, 466 (1955).
[90] I. Nagy, A. Arnau, P. M. Echenique, and E. Zaremba, Phys. Rev. B **40**, 11983 (1989).
[91] J. B. Malherbe and H. W. Alberts, Nucl. Instrum. Methods Phys. Res. **196**, 499 (1982).
[92] Ch. Eppacher, Ph.D. thesis, University of Linz, 1995).
[93] Th. Krist and P. Mertens, Nucl. Instrum. Methods Phys. Res. **218**, 790 (1983); **218**, 821 (1983).
[94] J. C. Eckardt, Phys. Rev. A **18**, 426 (1978).
[95] E. P. Arkhipov and Yu. V. Gott, Sov. Phys. JETP **29**, 615 (1969).